

RESEARCH

Open Access



Genomics guiding personalized first-line immunotherapy response in lung and bladder tumors

Jenifer Brea-Iglesias^{1,2}, María Gallardo-Gómez^{1†}, Ana Oitabén^{1,2†}, Martín E. Lázaro-Quintela¹, Luis León³, Joao M. Alves^{4,5}, Manuel Pino-González¹, Laura Juaneda-Magdalena¹, Carme García-Benito^{1,6,7}, Ihab Abdulkader⁸, Laura Muinelo³, Jesús M. Paramio^{9,10,11} and Mónica Martínez-Fernández^{1*}

Abstract

Background Immune checkpoint inhibitors (ICI) have revolutionized cancer treatment, particularly in advanced non-small cell lung cancer (NSCLC) and muscle-invasive bladder cancer (MIBC). However, identifying reliable predictive biomarkers for ICI response remains a significant challenge. In this study, we analyzed real-world cohorts of advanced NSCLC and MIBC patients treated with ICI as first-line therapy.

Methods Tumor samples underwent Whole Genome Sequencing (WGS) to identify specific somatic variants and assess tumor mutational burden (TMB). Additionally, mutational signature extraction and pathway enrichment analyses were performed to uncover the underlying mechanisms of ICI response. We also characterized HLA-I haplotypes and investigated LINE-1 retrotransposition.

Results Distinct mutation patterns were identified in patients who responded to treatment, suggesting potential biomarkers for predicting ICI effectiveness. In NSCLC, tumor mutational burden (TMB) did not differ significantly between responders and non-responders, while in MIBC, higher TMB was linked to better responses. Specific mutational signatures and HLA haplotypes were associated with ICI response in both cancers. Pathway analysis showed that NSCLC responders had active inflammatory and immune pathways, while pathways enriched in non-responders related to FGFR3 and neural crest differentiation, associated to resistance mechanisms. In MIBC, responders had alterations in DNA repair, leading to more neoantigens and a stronger ICI response. Importantly, for the first time, we found that LINE-1 activation was positively linked to ICI response, especially in MIBC.

Conclusion These findings reveal promising biomarkers and mechanistic insights, offering a new perspective on predicting ICI response and opening up exciting possibilities for more personalized immunotherapy strategies in NSCLC and MIBC.

Keywords Immune checkpoint inhibitors (ICI), HLA, Genomic mutation profile, Retrotransposition, LINE-1, TMB

[†]María Gallardo-Gómez and Ana Oitabén have contributed equally to this work.

*Correspondence:

Mónica Martínez-Fernández
monica.martinez@iisgaliciasur.es

Full list of author information is available at the end of the article



Background

Immune checkpoint inhibitors (ICI) are improving patient survival and enhancing available therapeutic options for different cancers. Their association with improved quality of life and longer life expectancy in advanced cancer patients, whose prior therapeutic options were limited, has positioned them as the standard first-line treatment for the management of several advanced tumors. Nevertheless, response rates to ICI remain below 20–40% and the mechanisms driving ICI response are yet to be understood.

High PD-L1 staining by immunohistochemistry has been the stratification criterion to undergo ICI therapy. However, it presents several pitfalls: first, conflicting evidence has been reported with some responders showing low PD-L1 staining and some non-responders with positive staining (due, for instance, to immune-excluded tumors) [1]. Second, its high heterogeneity, lack of standardization (with different calculation methods (i.e. TPS, CPS)), lax positivity threshold, and possible inter-pathologist bias lead to the administration of ICI to almost all candidate patients [2, 3]. The tumor mutational burden (TMB, defined as the number of non-synonymous mutations per megabase) has been also considered a candidate biomarker for ICI response, as somatic mutations can act as neoantigens that may favor tumor recognition by infiltrating T-cells during ICI treatment [4, 5]. However, TMB was originally calculated through whole-exome sequencing (WES), complicating its clinical implementation due to the need of sufficient input material (not always available in small biopsies) and specific technical equipment and expertise [6]. Despite the attempts to obtain TMB from targeted panels, the discrepancy of the results has prevented its clinical implementation.

But not only the quantity of neoantigens has been associated with ICI response, the quality of the neoantigens (immunogenicity) can impact on ICI response. Different sources of high-quality neoantigens have been recently proposed as ICI biomarkers, such as those generated by transposable elements (TE) that can be transcriptionally activated during cancer, which may explain why tumors with low TMB show good immunotherapy responses [7, 8]. Among TE, the Pan-Cancer initiative has identified LINE-1 retrotransposons (L1) as being particularly active in certain tumor types [9, 10]. Interestingly, most of the tumor-specific TE-chimeric transcripts derive from the LINE class [11] and analyzing how active L1 can impact ICI response remains a pending question. Parallel to neoantigen generation, antigen processing and presentation is a crucial aspect of antitumor immunity under checkpoint blockade, and the repertoire of the Human Leukocyte Antigen (HLA) has recently emerged as a major focus of biomarker discovery efforts [12, 13].

Thus, we have performed a comprehensive characterization of the genomic landscape of advanced lung and bladder primary tumors from patients treated with ICI in first line. First, lung cancer remains the leading cause of cancer morbidity and mortality worldwide [14]. Specifically, non-small cell lung cancer (NSCLC) represents 85% of lung cancer cases, and over 40% of patients are diagnosed at advanced stages, when surgical resection is not feasible, leading to a 5-year survival rate of just 9%. Second, in the case of urothelial carcinoma, also referred to as bladder cancer, in which 20–25% of patients present muscle invasive bladder cancer (MIBC) at diagnosis [15] and, although radical cystectomy is the standard treatment, it only provides a 50% 5-year survival rate [16]. In both cases, ICI have supported a new therapy paradigm representing the gold standard for metastatic NSCLC without an associated targeted therapy [17, 18], and very recently also for metastatic urothelial carcinoma in combination with enfortumab-vedotin [19], with several clinical trials analyzing its potential in neoadjuvant settings.

Therefore, effective predictive biomarkers represent an urgent need to identify those patients most likely to benefit from ICI therapy. After profiling the genome from NSCLC and MIBC patients treated with ICI in two real-world cohorts, we have identified specific somatic alterations and mutational signatures associated with ICI response. We have additionally evaluated (*) whether non-coding regions impact TMB calculation, (**) the presence of specific HLA-I haplotypes as relevant predictors of response to ICI, and the activation of L1 elements as potential high-quality neoantigens (***)

Methods

Patients' cohorts, response and survival

We included a total of 34 advanced NSCLC patients collected from Hospital Álvaro Cunqueiro (Complejo Hospitalario Universitario de Vigo, CHUVI, Spain) and Complejo Hospitalario Universitario de Santiago (CHUS, Santiago de Compostela, Spain). Considering that our main aim was to facilitate the prediction of ICI response in patients that are frequently multi-treated and start with the immunotherapy after progressing to several therapy lines, all patients were treated with ICI at first line, either alone or in combination with chemotherapy (Table 1). In this way, our genomic results are really impacted by the ICI treatment and not by the result of several therapy pressures, even when this restricted the number of candidate patients.

We characterized the mutation profile of 17 patients using whole genome sequencing (WGS) and evaluated L1 retrotransposition in 31 patients. Treatment-naive formalin-fixed paraffin-embedded (FFPE) primary tumor biopsies were collected and peripheral blood mononuclear

Table 1 Clinicopathological characteristics of the NSCLC cohort

	All patients (n = 34)	3 months after ICI		6 months after ICI		
		R (n = 22)	NR (n = 12)	R (n = 10)	NR (n = 14)	NA (n = 10)
<i>Sex</i>						
Female	9	4	5	3	6	0
Male	16	10	6	7	8	1
NA	9	8	1	0	0	9
<i>Age (median) (range)</i>						
	63 (43–78)	63 (51–77)	60 (43–78)	66 (51–76)	62 (43–78)	59
<i>Smoking status</i>						
Smoker	19	11	8	7	11	1
Former smoker	5	3	2	3	2	0
Never smoker	1	0	1	0	1	0
NA	9	8	1	0	0	9
<i>Histological subtype</i>						
ADC	16	8	8	6	10	0
SCC	8	5	3	3	4	1
NA	10	9	1	1	0	9
<i>Tumor stage</i>						
IIIC	2	1	1	1	1	0
IVA	6	6	0	4	2	0
IVB	9	1	8	1	8	0
NA	17	14	3	4	3	10
<i>Treatment scheme</i>						
ICI	31	20	12	8	14	9
ICI-CT	3	2	0	2	0	1

ADC adenocarcinoma, CT chemotherapy, ICI Immune checkpoint inhibitors, NR non-responder, R responder, SCC squamous cell carcinoma

cells (PBMCs) from the same NSCLC patients were used as germline control. Since intra-tumor heterogeneity has an important impact in the pathological diagnosis, even more in tumors where only small-size biopsies are available such as advanced lung cancer, our pathologists have ensured that the FFPE biopsies included had a minimum tumor content of at least 60%. Immunotherapy response was evaluated by computed tomography scan at 3 and 6 months after the first dose. Durable response was evaluated according to the response at 6 months.

Furthermore, we included 26 MIBC patients involved in various clinical trials for neoadjuvant ICI treatment evaluation at Hospital “12 de Octubre” (Madrid, Spain) (Table 2). We analyzed a sub-cohort of 10 patients from the ABACUS clinical trial [20] using WGS and the 26 patients for L1 activation. FFPE primary tumor biopsies were obtained and response to ICI was evaluated at cystectomy. Post-ICI FFPE tumor samples were also acquired at cystectomy for 4 out of the 10 patients subjected to WGS.

Table 2 Clinicopathological characteristics of the MIBC cohort

	All (n = 26)	R (n = 19)	NR (n = 7)
<i>Sex</i>			
Female	4	3	1
Male	8	4	4
NA	14	12	2
<i>Age (median) (range)</i>			
	70 (51–82)	66 (51–82)	70 (68–80)
<i>Smoking status</i>			
Smoker	5	3	2
Former smoker	3	2	1
Never smoker	4	2	2
NA	14	12	2
<i>Histological subtype</i>			
Flat urothelial	9	5	4
Papillary urothelial	3	2	1
NA	14	12	2

NR non-responder, R responder

In both cohorts, patients' characteristics among the whole set of patients and the subset undergoing WGS are exactly the same. Patients with stable disease, partial response, and complete response were classified as responders (R), while non-evaluable patients (*exitus*) or patients with disease progression at the time of evaluation were considered non-responders (NR). Overall survival (OS) was defined as the time from treatment initiation to the time of death, while progression-free survival (PFS) was defined as the time from treatment initiation to the time of progression or death, whichever is earlier. The study was conducted with appropriate authorization from the Galician Regional Research Ethics Committee (2019/046) and from the Ethics Committee from Hospital "12 de Octubre" (17/094) following the Helsinki Declaration of 1975 and all patients signed informed consent approving their participation.

Sample preparation and WGS

We isolated genomic DNA from FFPE samples from NSCLC and MIBC tumors using QIAamp DNA FFPE Tissue kit (Qiagen). PBMCs from NCLC patients were obtained by Ficoll density gradient from a blood sample drawn before the first ICI dose (baseline). We extracted DNA from PBMCs with the QIAamp DNA Blood Mini kit (Qiagen), according to manufacturer's protocol, as germline control. We checked DNA quality using Qubit dsDNA BR Assay Kit in Qubit 4.0 (Thermo Fisher) and quantified the total yield and gDNA ScreenTape Analysis in a 4200 TapeStation system (Agilent Technologies) to assess the DNA integrity. Samples were sequenced in an external service (Macrogen) with Illumina Truseq Nano DNA Library in a NovaSeq6000 (Illumina) at 150 bp PE.

WGS data processing

We assessed the quality of raw WGS data with *FastQC* [21]. We next mapped the sequencing reads from both tumor and PBMC samples to the GRCh37/hg19 reference genome using the Burrows-Wheeler Aligner (*BWA-mem* v0.7.17) [22, 23]. Afterwards, we used *Samtools* v1.9 [24] to sort the aligned reads and to index the generated bam files. Duplicated reads were marked with *Picard Bammarkduplicates* [25]. Finally, we used *Base Quality Score Recalibration* (BQSR) from the *Genome Analysis Tool Kit* (GATK) v4.1.7.0 [26] to correct quality score bias, following the best practices guidelines [27].

SNVs and INDELS calling

Before variant calling, we estimated cross sample contamination using GATK's *GetPileupSummaries* and *CalculateContamination*, as well as the genomAD resource obtained from the GATK bundle (<https://console.cloud.google.com/storage/browser/gatk-best-practices/somat>

[ic-b37;tab=objects?prefix=](#)). Next, we used *Mutect2* v0.7.17 [28] for calling SNV and indels. For NSCLC, we performed cross sample contamination in paired-sample mode, using the PBMCs data as germline control, while for pre-treatment MIBC samples it was performed in tumor-only mode. For the post-treatment samples analysis, we used the matching pre-treatment sample as control. We next applied *FilterMutectCalls* with standard parameters to remove low quality variants, considering the estimates from both *CalculateContamination* and *LearnReadOrientationModel*, which identifies paraffin related artifacts. Those variants selected by *FilterMutectCalls* in at least two patients were considered artifacts and discarded from further analyses. The remaining variants were finally annotated with the *Ensembl Variant Effect Predictor* (VEP) v100.2 [29]. We identified likely pathogenic variants according to *SIFT* [30] and *Polyphen* [31] scores and used *vcf2maf* v1.6.21 [32] to transform the VCF files to MAF format. We used the *mafTools* R package v2.16.0 [33] for downstream analyses and visualization purposes.

SNVs and INDELS custom filtering

To further remove low quality variants and potential artifacts for mutational signatures extraction and functional enrichment, we additionally removed mutations occurring in the following genome conflicting regions according to UCSC Genome Browser: (i) sites present in the NCBI track dbVar Curated Common SVs Conflicts with Pathogenic (DbVarConflict), which includes common structural variants that overlap with structural variants with ClinVar annotation [34]; (ii) variants present in the regions of the ENCODE blacklist subtrack, which contains a set of problematic regions due to a high ratio of multi-mapping to unique mapping reads and high variance in mappability due to repetitive elements [35]; (iii) sites present in the database of fragile sites in human chromosomes (HumCFS) [36]; and (iv) variants overlapping with the Genome-In-A-Bottle (GIAB) giabCallConflict track set, that contains a set of regions where it is difficult to make a confident call, due to low coverage, systematic sequencing errors and local alignment problems [37].

TMB and the ratio of non-synonymous vs. synonymous substitutions (dN/dS)

We determined the TMB of each tumor sample as follows: (i) the genomic TMB was calculated as the 10-base logarithm of the number of total variants divided by the total genome size, while (ii) the coding TMB was calculated as the 10-base logarithm of the number of non-synonymous variants located in exonic regions divided by 10^6 .

Regarding dN/dS analysis and MIBC post-therapy variant analysis, we decided to reduce even more the noise from low frequency and unreliable calls, so we removed variants with less than 10 supporting reads in either the tumor or the corresponding PBMC sample, variants that were called in the PBMC sample, and variants with less than 0.075 variant allele frequency (VAF) in the tumor sample. Additionally, as variant calling in MIBC pre-treatment samples was performed in tumor-only mode, we discarded variants with a VAF greater than 0.45 to rely only on subclonal variants.

Afterwards, these filtered variant sets were used to estimate the dN/dS score for each tumor sample to infer selection pressure in protein-coding genes through *dNdScv*, which applies a maximum likelihood approach to quantify selection patterns [38]. We selected dN/dS because it offers a broad, well-established and interpretable framework for identifying positive and negative selection in coding regions.

Single-base substitution (SBS) signature extraction and assignment

To study mutational signatures, we used the *trinucleotideMatrix* function from *maftools* to extract the immediate bases flanking the mutated site and to classify them into 96 classes depending on the combination of the trinucleotides. Then, we applied *extractSignatures* function to decompose the matrix into n signatures. The number of signatures was chosen based on the value at which Cophenetic correlation, which measures the goodness of fit of the non-negative matrix factorization model, drops significantly (which can be calculated through *estimateSignatures* and *plotCophenetic* functions). Finally, we used *compareSignatures* function cosine similarity to detect the best similarity to COSMIC database known signatures [39].

CNV calling

We identified the copy number variants (CNV) of NSCLC tumor samples with the purity and ploidy estimator (*PURPLE*) [40] in the paired-sample mode under default parameters, using tumor and PBMCs bam files together with the SNV and indel calling as input. We determined different CNV regions between responder and non-responder patients, together with the genes contained in each aberrant region with *GISTIC2.0* [41], using the CNV segments in each sample. The identification of differentially amplified/deleted regions was based on a G-score assigned to each of them, depending on their amplitude and their alteration frequency across the set of samples of each group. A q -value false discovery rate of 25% was set to call a significant region and then the window with the greatest amplitude and frequency was

considered the “peak” of the region. We determined the boundary of each peak by the *RegBoulder* algorithm implemented in *GISTIC2.0*, with a 95% confidence level to include target genes within each region [41].

Enrichment analysis

We performed an enrichment analysis using *enrichR* R package [42, 43], an interface to the Enrichr database hosted at <https://maayanlab.cloud/Enrichr/>. This tool assesses whether our differentially mutated gene sets were enriched in specific biological/molecular functions by measuring the statistical significance (Fisher exact test) of the overrepresentation of a gene set in a specific list of genes. We selected the following databases: Human MSigDB collections (including MSigDB_Hallmark_2020, MSigDB_Oncogenic_Signatures, and MSigDB_Computational) [44, 45], BioPlanet_2019 [46], KEGG_2019_Human [47, 48], WikiPathways_2019_Human [49, 50], GO_Molecular_Function_2018, and GO_Biological_Process_2018 [51, 52], ChEA_2016 [42] and TRANSFAC_and_JASPAR_PWMs [53].

HLA-I haplotyping and HLA LOH analysis

To identify HLA-I haplotypes we applied *LILAC* [54], a tool which determines HLA-I germline alleles by aligning the sequencing reads to HLA-A, HLA-B and HLA-C regions which are present in the IMGT/HLA database [55]. Following their recommended pipeline, we first performed an “elimination” phase, removing allele candidates that are clearly not present in the sample, and an “evidence” step, which selects the best solution based on the observed reads amongst the whole set of possible HLA-I alleles. For the NSCLC cohort, we used both tumor and PMBCs bam files as input, together with the somatic variants (SNVs, INDELS, and CNA). For the MIBC cohort, we used tumor bam files and somatic variants (SNVs and INDELS). We also determined Loss of Heterozygosity (LOH) events affecting HLA haplotypes (HLA^{LOH}) for NSCLC patients when the copy number estimated by *PURPLE* [40] (see Methods Sect. 2.6) was less than 0.5.

Neoantigen prediction

To get insights into the quantity and quality of neoantigens associated to ICI response, we performed a preliminary neoantigen prediction analysis of the top-most frequent exclusively mutated genes in responders and non-responders for both NSCLC and MIBC patients. We used the netMHCpan-4.0 tool (v.4.1) [56] to obtain the binding affinity of all possible 6 to 14-mer wild-type and aberrant peptides to the most representative HLA alleles (HLA-A1, HLA-A2, HLA-A3, HLA-A24, HLA-A26, HLA-B7, HLA-B8, HLA-B15, HLA-B27,

HLA-B39, HLA-B40 and HLA-B58). Peptide antigenicity was assessed by the eluted ligand rank (EL_Rank), a rank-based score to estimate the likelihood that a peptide will be naturally processed and presented by MHC molecules. The score is given as a percentile rank, where a lower EL_Rank indicates a stronger or more likely binder. Peptides with a rank between 0.5–2% were considered low-binders and those with a rank lower than 0.5% were selected as strong binders to HLA alleles and therefore considered potential neoantigens.

LINE-1 retrotransposition rate quantification by RetroTest

To quantify the amount of LINE-1 (L1) somatic insertions, we applied the RetroTest targeted sequencing method [57], based on the use of probes that capture the unique sequence downstream of the 124 most active L1 elements of the human genome [9]. RetroTest library construction and bioinformatic processing were performed following the recommended approach [57].

Statistical analyses

We performed survival analyses using OS and PFS with censoring at the date of the last follow-up if a patient was alive and without disease progression. We combined clinical variables (sex, age, smoking habits and PD-L1

staining) in a multivariate Cox proportional hazards ratio (HR) model with PFS as response variable, with the *coxph* function from the *survival* v3.5.7 R package. We estimated survival curves using the Kaplan–Meier method and compared them with the log-rank test. We assessed the significance between the TMB, the L1 insertion rate and the presence of HLA^{LOH} between responder and non-responder patients with the non-parametric Wilcoxon rank sum test (*p*-value threshold of 0.05). For multi-testing correction, we computed FDR values from nominal *p*-values using the Benjamini–Hochberg method.

Results

Clinic-pathological characteristics of ICI response

We collected FFPE tumor biopsies at baseline before the start of first line ICI therapy from 34 advanced NSCLC patients with a median age of 63 years old, mostly males and tobacco smokers (Table 1). Both FFPE tumor samples and matching PBMCs from 17 patients underwent WGS (n=34), and RetroTest was applied to 31 FFPE tumor biopsies (Fig. 1A). Most patients received single-agent ICI therapy (anti-PD1 pembrolizumab, n=31), while three of them were treated with ICI in combination with chemotherapy at first line. Our cohort

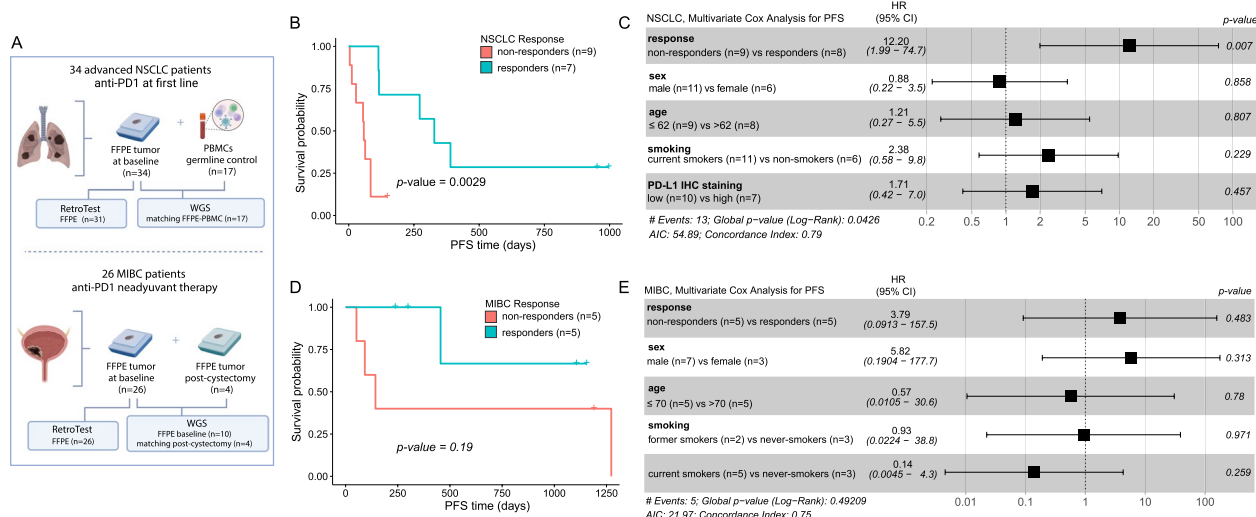


Fig. 1 Overview of the NSCLC and MIBC cohorts. **A** Schematic representation of the two cohorts. For NSCLC patients treated with anti-PD1 at first line, treatment-naïve FFPE tumor biopsies were collected for 34 patients and matching PBMCs as germline controls were collected from 17 patients. For MIBC patients who received anti-PD1 neoadjuvant therapy, treatment-naïve FFPE tumor biopsies were obtained for 26 patients; plus, matching FFPE tumor samples were obtained post-cystectomy for 4 patients. **B** Kaplan–Meier curves for PFS with respect to ICI response for NSCLC patients subjected to WGS. Patients were grouped into responders and non-responders to ICI as evaluated by CT scan 3 months after the first anti-PD1 dose. Log-rank test was used to calculate the *p*-value. **C** Forest plot for the HR of response, sex, age, smoking status and PD-L1 TPS with respect to PFS in NSCLC patients subjected to WGS, obtained by multivariate Cox regression. The error bars indicate 95% CI for the HR. **D** Kaplan–Meier curves for PFS with respect to ICI response for MIBC subjected to WGS. Patients were grouped into responders and non-responders to anti-PD1 evaluated at the time of cystectomy. Log-rank test was used to calculate the *p*-value. **E** Forest plot for the HR of response, sex, age and smoking status with respect to PFS in MIBC patients subjected to WGS, obtained by multivariate Cox regression. The error bars indicate 95% CI (confidence interval) for the HR

consisted mainly of adenocarcinoma histology (n=16). All patients presented high PD-L1 staining (TPS \geq 50%, median TPS of 80%). Responder patients (R) showed higher PFS (log-rank *p*-value=0.0029, Fig. 1B) and OS (log-rank *p*-value=0.011, Supplemental Fig. 1A) than non-responder patients (NR). We evaluated whether any clinical variables were associated with improved PFS. Although non-significant, low PD-L1 staining (TPS \leq 80%) and smoking at the time of diagnosis showed an unfavorable tendency regarding PFS. Neither sex, nor age, reported a statistically significant association with PFS (Fig. 1C). Only ICI response showed a statistically significant impact on PFS.

In the case of MIBC patients, we collected FFPE tumor biopsies from 26 patients that received ICI as neoadjuvant therapy before radical cystectomy in the context of clinical trials (Table 2). All FFPE baseline treatment-naïve tumor tissues were subjected to RetroTest (n=26), and 10 pre-treatment tumor samples and 4 matching post-cystectomy bladder tissue underwent WGS (Fig. 1A). Patients showed a median age of 70 years old. Most were male and tobacco smokers, and most tumors showed urothelial histology (n=9). Response to ICI therapy was evaluated after cystectomy and did not have impact in neither PFS nor OS (log-rank *p*-values 0.19 and 0.99, respectively, Fig. 1D, Supplemental Fig. 1B). Neither response, sex, age, nor smoking habits reported a statistically significant association with PFS (Fig. 1E), confirming the same results as in the original ABACUS clinical trial [20].

NSCLC mutation profiling and TMB in ICI response

We identified an average of 37,432 (9315–104,704) somatic variants (SNVs and INDELS) per sample in a total of 36,063 genes. To identify a list of potential candidate biomarkers for ICI response, we selected genes mutated in, at least, two patients of each group (i.e., mutated in two or more responder patients and not mutated in any of the non-responder patients, or vice versa). We found a total of 1,216 genes exclusively mutated in R patients and 1,748 genes exclusively mutated in NR patients (Supplemental Tables 1, 2). We found that *ATP6V1E1*, *RP11-397E7.1* and *RP11-69I8.2* were the most mutated genes exclusively among R (found in 35.3%), while *FAM63B*, *MYH4*, *OR10D3*, *PROZ*, *RMND1*, *RNU6-743P*, *RP11-122G11.1*, and *RP4-715N11.2* were the top among NR (35.3%).

When focusing on potentially pathogenic variants, we found an average of 92.88 variants per patient (16–316) in a total of 1,316 genes. We did not find differences on TMB, tumor purity, or type of mutation between R and NR (Fig. 2A). The most mutated genes with pathogenic variants were *TP53* (82% of the patients), *CSMD3* (47%),

and *KRAS* (29%), found both in R and NR. We detected 26 genes harboring pathogenic variants exclusively in R, while 34 genes were exclusively mutated in NR (Supplemental Tables 3, 4, complete list of variants in Supplemental Table 5). *PIEZO* was found to be exclusively mutated and the most mutated gene among R (50%), while *MT-CO3* gene was exclusive and the most mutated in NR (33.3%).

Afterwards, the COSMIC mutational signatures were extracted from the whole set of variants in both R and NR patients. Signatures COSMIC_4 (“exposure to tobacco (smoking) mutagens”) and COSMIC_5 were the most-common mutational signatures assigned to both R (cophenetic correlation=0.982) and NR (cophenetic correlation=0.989) (Fig. 2B, C). Based on the dN/dS ratio, we evaluated the mutation selection patterns between responder and non-responder patients. We did not find evidence of positive or negative selection related to response in the different mutation types, although R showed a slight enrichment in missense mutations than NR (Fig. 2D).

We next explored the relationship between CNAs and ICI response in our cohort. We detected 13 patients with whole genome duplication (WGD), with an average ploidy of 3.37 (Fig. 2A). Moreover, responder patients showed 66 regions with focal CNAs that were statistically significant (FDR *q*-value<5%), of which 21 were exclusively found in R (Fig. 2E, Supplemental Table 6). Interestingly, we found two events in *MDM2* with pathogenic variants exclusively found in R. In NR patients, we observed a total of 227 regions with statistically significant CNAs (FDR *q*-value<5%), of which 179 were exclusively present in NR patients (Fig. 2F, Supplemental Table 7). The pathogenic variants found exclusively in NR correspond to events overlapping *PTPRU* and *ARPP21*.

Finally, we compared the extent to which TMB can predict ICI response in our real-world cohort following two different approaches: first, we determined the TMB for each tumor sample as “genomic TMB” considering the number total of variants divided by the total genome size. Second, “the coding TMB” was calculated based on the number of non-synonymous variants located exclusively in exonic regions. In both cases, no statistically significant differences were observed between the TMB of NR and R patients (Fig. 2G).

MIBC mutation profiling and TMB in ICI response

We identified an average of 199,221 (117,661–456,401) somatic variants (SNVs and INDELS) per sample in MIBC FFPE tumor tissue at baseline, in a total of 63,167 genes. The majority of these variants have an allele frequency below heterozygosity (Supplemental Fig. 2A), indicating a small amount of non-filtered germline variants. As

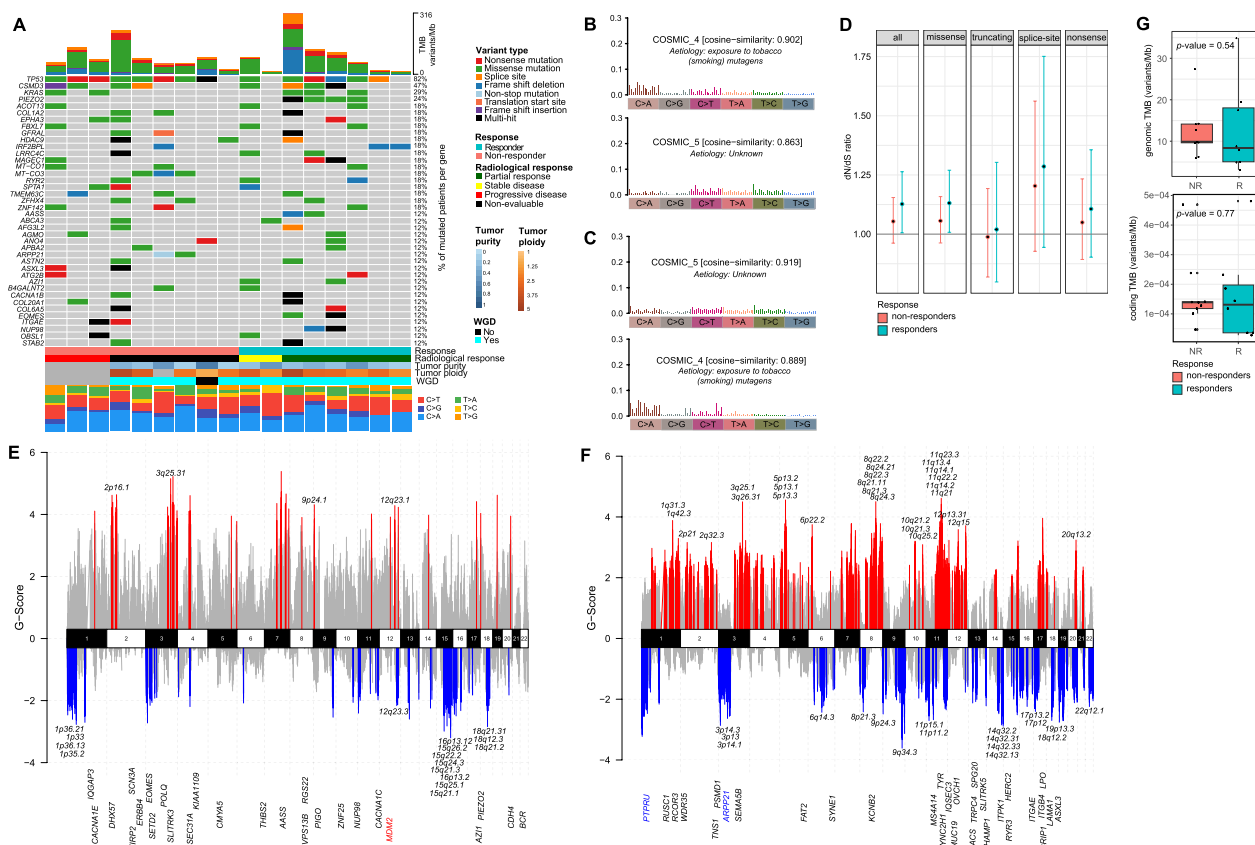


Fig. 2 Somatic variants landscape and TMB in NSCLC patients. **A** Oncoplot showing the top-40 most frequently mutated genes harboring probably pathogenic variants in the cohort of NSCLC patients. **B** Most common COSMIC mutational signatures for responder patients. **C** Most common COSMIC mutational signatures for non-responder patients. **D** Maximum Likelihood Estimation (MLE) of the dN/dS ratio for responder and non-responder patients considering different sets of variants. **E** Copy number variants profile showing the 66 significantly amplified (red) or deleted (blue) cytobands in responder patients. Those 21 cytobands exclusively altered in responder patients are labelled with their cytoband ID. Genes with probably pathogenic variants found exclusively in responder patients are shown sorted by genomic location. **F** Copy number variants profile showing the 227 significantly amplified (red) or deleted (blue) cytobands in non-responder patients. From the 179 cytobands exclusively altered in responder patients, the top-50 are labelled with their cytoband ID. Genes with probably pathogenic variants found exclusively in non-responder patients are shown sorted by genomic location. **G** Boxplots of the TMB calculated considering only variants in coding regions (left) and of the TMB calculated considering all variants in genomic regions (right) with respect to immunotherapy response. Differential p -value was derived by the Wilcoxon rank-sum test. The central mark represents the median, with 25th and 95th percentiles at the box, 5th and 95th percentiles at the whiskers and minima and maxima noted by dots.

before, we selected genes exclusively mutated in at least two patients from each group (R vs. NR) to identify genes potentially associated with ICI response. A total of 5067 genes were exclusively mutated in R patients, of which 77 genes were mutated in all R (Supplemental Table 8). On the other hand, NR patients showed 721 genes exclusively mutated (Supplemental Table 9). When considering just pathogenic variants, we found an average of 675.5 (137–2,415) variants per sample in baseline samples, in a total of 4215 genes. The most mutated genes were *TP53* (70%) and *ZFH4* (60%) (Fig. 3A). To identify potential biomarkers for neoadjuvant ICI response, we selected the exclusively mutated genes with pathogenic variants. A total of 614 genes were exclusively mutated in R

patients (Supplemental Table 10) and 24 genes were only mutated in NR (Supplemental Table 11) (Supplemental Table 12 for the complete list of variants). We found that *PKHD1* gene harbored pathogenic variants in all the R patients and that *HEATR5B* and *WDR36* were exclusively mutated in NR patients.

Using all identified variants, we next extracted the COSMIC mutational signatures in R (cophenetic correlation=0.997) and NR (cophenetic correlation=0.956) patients. COSMIC_5 was a common signature to both groups (Fig. 3B, C). In contrast, COSMIC_13 (*APOBEC Cytidine Deaminase*) was only found in R (Fig. 3B), while COSMIC_3 (*defects in DNA–DSB repair by HR*) was exclusively identified in NR (Fig. 3C).

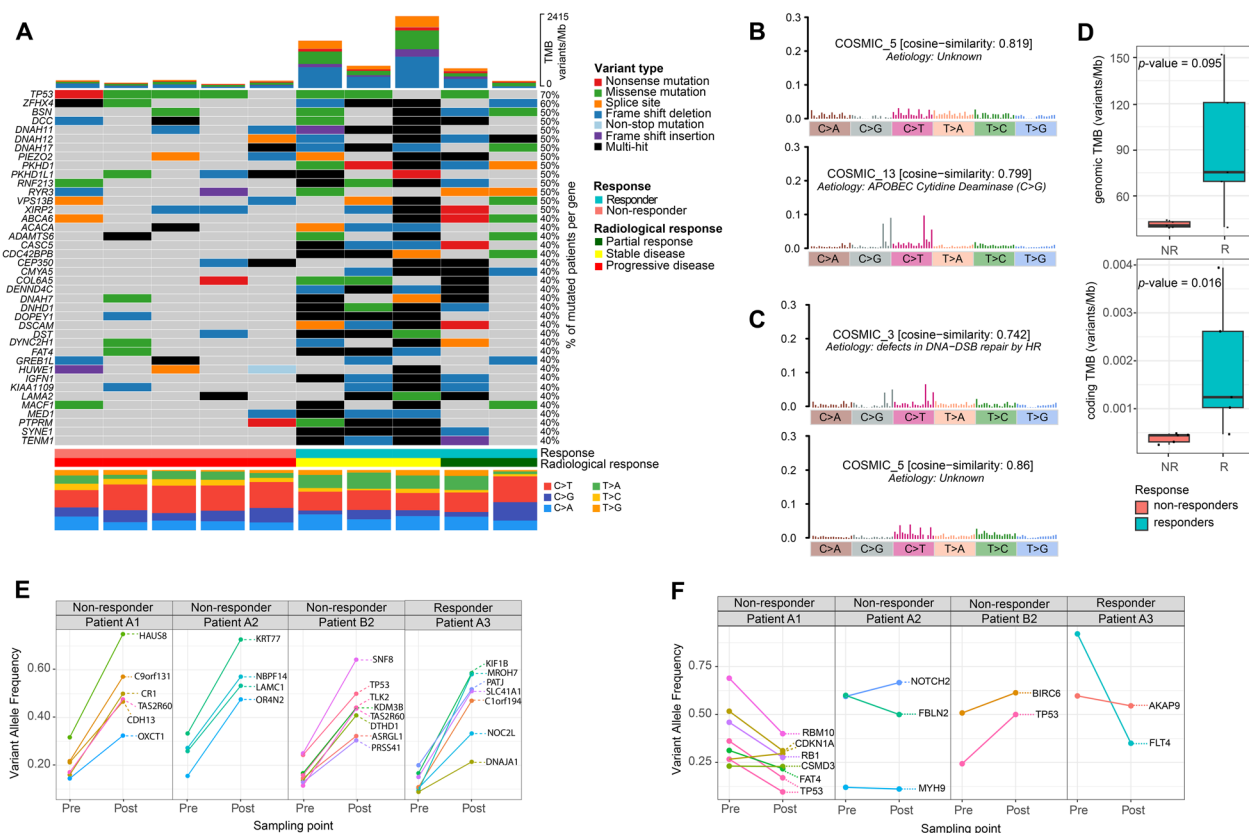


Fig. 3 Somatic variants landscape and TMB in MIBC patients treated with neoadjuvant immunotherapy. **A** OncoPrint showing the top-40 most frequently mutated genes harboring probably pathogenic variants in the cohort of MIBC patients. **B** Most common COSMIC mutational signatures for responder patients. **C** Most common COSMIC mutational signatures for non-responder patients. **D** Boxplots of the TMB calculated considering all variants ("genomic TMB") and of the TMB calculated considering only variants in coding regions ("coding TMB") with respect to immunotherapy response. Differential p-value was derived by the Wilcoxon rank sum test. The central mark represents the median, with 25th and 95th percentiles at the box, 5th and 95th percentiles at the whiskers, and minima and maxima noted by dots. **E** Variant allele frequencies of genes with exonic variants that were shared between a pair of pre- and post-anti-PD1 neoadjuvant therapy. **F** Variant allele frequency shift of exonic variants present in bladder cancer driver genes

We next assessed the predictive potential of TMB calculated following the two different approaches explained above. Interestingly, R patients presented substantially higher TMB compared to NR. However, this difference was only statistically significant when considering coding variants (p -value = 0.016) (Fig. 3D).

Changes in the mutational profiling during ICI treatment in MIBC

In four MIBC patients, besides the baseline treatment-naïve samples we also obtained a bladder tissue sample from the radical cystectomy after the treatment. Three of the patients were non-responders, showing progressive disease at the time of cystectomy while one showed partial response. We investigated the changes in the mutation profile in the bladder before and after the treatment and reported that post-ICI samples generally have higher SNV count than pre-ICI samples

(Supplemental Fig. 2B). Next, we focused on the gene identities already altered in the pre-ICI sample. Specifically, we analyzed variant allele frequency (VAF) shifts of the mutations shared between the pairs of matching pre- and post- samples. When considering all variants, we did not find a clear VAF shift pattern between pre- and post-ICI treatment (Supplemental Fig. 2C), even when only considering exonic/coding regions (Supplemental Fig. 2D). Nevertheless, we detected 25 genes with variants whose VAF substantially increased in post-treatment samples (Fig. 3E). When focusing exclusively on MIBC driver genes, we did not find a common pattern, and all the exonic variants that changed their VAF before and after the treatment were patient exclusive. The only gene with VAF changes in two NR patients was *TP53*: one NR patient presented two different *TP53* variants with lower VAF in the post-treatment sample, while another NR harbored a *TP53*

mutation positively selected (VAF from 0.25 to 0.5) after ICI therapy (Fig. 3F).

Gene pathways implicated in ICI response in NSCLC and MIBC

After assessing that the enriched pathways on the aggregated set of all mutated genes in each group of patients were similar (Supplemental Fig. 3, Supplemental File 1), we performed an enrichment analysis focusing on genes exclusively mutated in only one of the groups (R vs. NR). In the NSCLC cohort, we found that immune related pathways including inflammatory response, and some related to Ras, T-cell receptor/Ras pathway, activation of Ras in B-cells were enriched in R (Supplemental Fig. 4A, Supplemental File 2), while the Ras-independent pathway in NK cell-mediated cytotoxicity, neural crest differentiation, PI3K/Akt signaling pathway and FGFR3 and FGFR4 ligand binding and activation pathways appeared enriched in NR (Supplemental Fig. 4B, Supplemental File 3). When focusing on pathogenic variants, we observed that R were enriched

in several ERBB4 related pathways such as PI3K events in ERBB2 signaling, signaling by ERBB4 or down regulation of ERBB4 signaling (Fig. 4A, Supplemental File 4). In the case of NR, we detected processes related to cell signaling with an important role of integrins, or ECM-receptor interaction (Fig. 4B, Supplemental File 5). In addition, adaptive immune system and antigen presentation (folding, assembly, and peptide loading of MHC class-I proteins pathway) were also altered among NR patients. It is worth mentioning that we detected variants affecting other antigen presentation genes more frequently in NR, specifically in genes such as *HERC2*, *PSMD1*, *PSMA6*, and *B2M*. Intriguingly, we realized that SNVs in *B2M* were also amplified in two of the patients.

In the MIBC cohort, we found no significantly enriched pathways (Supplemental Fig. 4C, D, Supplemental Files 6 and 7), suggesting a high variability in the cohort. When focusing only on pathogenic variants, we found Double-strand break repair pathway, integrins in angiogenesis and interaction between L1-type

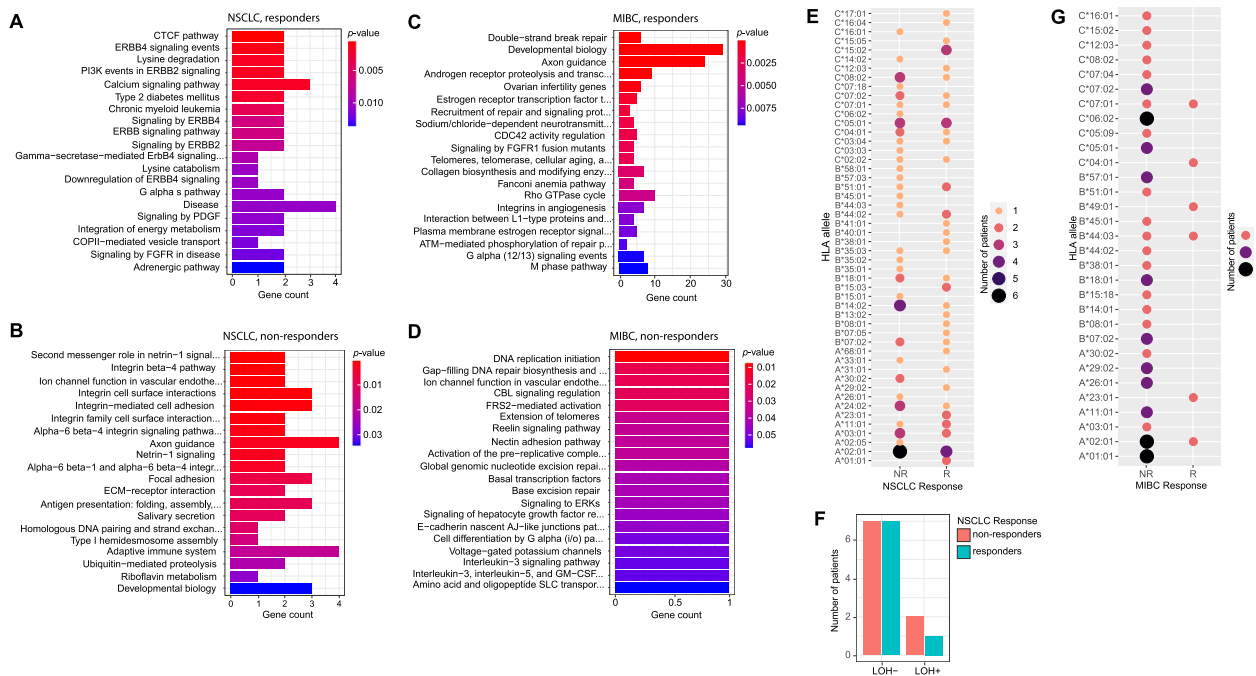


Fig. 4 Functional enrichment of somatic variants and HLA typing in responder and non-responder patients. **A** Barplot of the pathway enrichment analysis based on the 26 genes that contain potentially pathogenic variants exclusive of NSCLC responder patients. **B** Barplot of the pathway enrichment analysis based on the 34 genes that contain potentially pathogenic variants exclusive of NSCLC non-responder patients. **C** Barplot of the pathway enrichment analysis based on the 614 genes that contain potentially pathogenic variants exclusive of MIBC responder patients. **D** Barplot of the pathway enrichment analysis based on the 24 genes that contain potentially pathogenic variants exclusive of MIBC non-responder patients. Enrichment p-values were calculated with the Fisher exact test. **E** HLA-I haplotypes repertoire for NSCLC patients. The bubble size and color indicate the number of patients presenting each specific haplotype. **F** HLA loss of heterozygosity (LOH) status among responder and non-responder NSCLC patients. A patient was considered positive for HLA^{LOH} if the copy number status estimation for the HLA locus was lower than 0.5. **G** HLA-I haplotypes repertoire for MIBC patients. The bubble size and color indicate the number of patients presenting each specific haplotype

proteins and ankyrins enriched in R patients (Fig. 4C, Supplemental file 8). With respect to NR patients, we did not find any statistically significant altered pathways, since all the pathways were only enriched by one gene (Fig. 4D, Supplemental File 9), indicating again a huge variability among patients.

HLA-I haplotypes repertoire and neoantigen prediction in immunotherapy response

Since cancer biology and ICI response are intimately related to immune processes such as antigen presentation, we next explored the HLA-I locus complexity in both cohorts.

In the NSCLC cohort, the most common haplotype was the HLA-A*02:01, present in four R and in six NR patients (Fig. 4E). With respect to ICI response, we found several HLA-I haplotypes that were exclusive to R patients, with HLA-A*01:01, HLA-A*23:01, HLA-B*15:03, and HLA-C*15:02 present in more than one patient. In the case of NR patients, HLA-A*30:02 resulted the only exclusive haplotype, present in two patients, while the alleles HLA-A*02:01 and HLA-B*14:02 were the most common haplotypes among NR, although non-exclusive (Fig. 4E). Based on our previous results, we analyzed if HLA loss of heterozygosity occurred more frequently in NR patients, finding that HLA^{LOH} was not statistically significantly higher in NR patients (p -value = 1, Fig. 4F).

For the MIBC cohort, we identified a higher heterogeneity of HLA-I haplotypes in NR patients, without any common haplotype (Fig. 4G). Interestingly, when focusing on exclusive haplotypes, HLA-C*06:02 and HLA-A*01:01 appeared exclusively in three NR patients, while HLA-B*49:01 and HLA-A*23:01 were exclusive for R patients (Fig. 4G).

Then, we applied the neoantigen prediction to the top-most exclusively mutated gene of NSCLC responders (*PIEZO2*) vs. non-responders (*MT-CO3*), and to those of MIBC exclusive of responders (*PKHD1*) vs. non-responders (*HEATR5B* and *WDR36*). We have shown that mutated genes generate more potential neoantigen peptides (EL_Rank < 0.5) than wild-type genes (Wilcoxon rank-sum test p -value = 0.0476).

In NSCLC, the peptides generated by mutations in *PIEZO2*, the most frequent exclusively mutated gene in responder patients, tend to bind HLA with stronger affinity than those peptides generated by mutations *MT-CO3*, the most frequently mutated gene in non-responder patients, although not reaching the statistical significance (Wilcoxon rank-sum test p -value = 0.186, Supplemental Fig. 5A). Interestingly, neoantigens derived from *PIEZO2* have statistically significant stronger affinity for

HLA-A*01:01 (Wilcoxon rank-sum test p -value = 0.0357, Supplemental Fig. 5B), and such HLA allele is exclusive of our NSCLC responder patients (Fig. 4E).

With respect to MIBC, we have shown that peptides derived from *PKHD1* variants, exclusively mutated in all responder patients, bind to HLA with stronger affinity than those peptides generated by *HEATR5B* and *WDR36* the most frequently mutated gene in non-responder patients (Wilcoxon rank-sum test p -value = 0.0002, Supplemental Fig. 5C). It is important to note that variants in *PKHD1*, *HEATR5B* and *WDR36* produce translation frameshifts, generating a high neoantigen load compared to the single aminoacid substitutions produced by *PIEZO2* and *MT-CO3* mutations.

Therefore, our results indicate that genes that are exclusively mutated in responder patients generate more amounts of neoantigen peptides and with a higher potential neoantigen activity, compared to peptides derived from exclusively mutated genes in non-responders.

LINE-1 (L1) role on ICI response

Next, we evaluated if L1 activity showed any association with TMB and/or ICI response according to the WGS data in both cohorts. In NSCLC, we did not find a statistically significant correlation between TMB and L1 activation (p -value = 0.37, Supplemental Fig. 6A, B). We also detected that L1 activation was not statistically significantly different between R and NR patients (p -value = 0.72, Fig. 5A). In the case of MIBC, we found a significantly positive correlation between the TMB and L1 activity (p -value = 0.013, Supplemental Fig. 6C, D). Interestingly, L1 activation was clearly higher in R patients, albeit not statistically significant (p -value = 0.09, Fig. 5B).

Based on these results, we decided to validate them by specifically determining L1 activity in larger cohorts using RetroTest [57]. We evaluated the impact of ICI response in patients' prognosis for a larger NSCLC cohort comprising 31 patients (Table 1). First, we confirmed that R patients showed better OS and PFS (log rank p -values of 0.002 and < 0.0001, respectively, Fig. 5C). Moreover, patients with durable response (6 months) also showed better OS (p -value = 0.002) and PFS (p -value < 0.0001) (Supplemental Fig. 6E). For MIBC, we did not have access to the patients' follow-up after the cystectomy to perform survival analyses. When analyzing L1 retrotransposition in these NSCLC patients, we found that patients with squamous tumors showed statistically higher L1 activity than those with adenocarcinomas (p -value = 0.032, Fig. 5D), while current smokers showed higher activation than former smokers (p -value = 0.049, Fig. 5E). Finally, when we evaluated L1 activity with respect to ICI response, we detected that 45.16% of patients showed

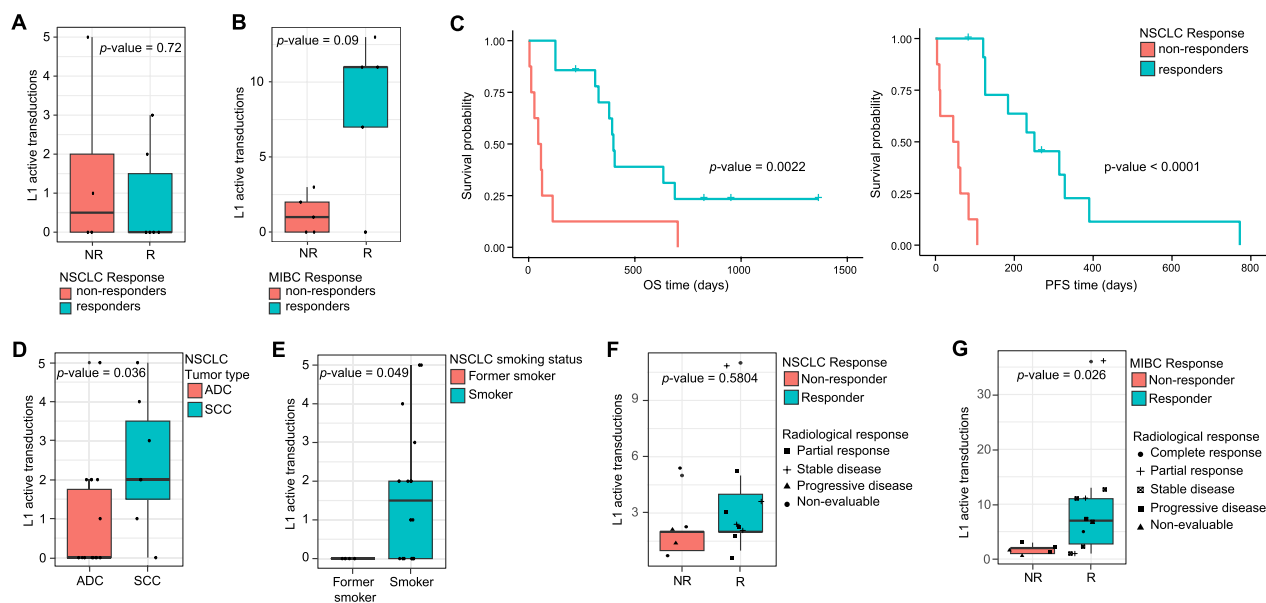


Fig. 5 Evaluation of L1 activation measured by RetroTest (L1 active transductions were calculated as the number of TD2 per sample) in NSCLC and MIBC patients treated with ICI. **A** Boxplot of L1 activation with respect to immunotherapy response in the cohort of NSCLC patients with WGS data ($n=17$). **B** Boxplot of L1 activity with respect to immunotherapy response in the cohort of MIBC patients with WGS data ($n=10$). **C** Kaplan–Meier curves for OS (left) and PFS (right) according to ICI response in NSCLC patients. The log-rank test was used to derive the p -values. **D** Boxplot of L1 activation based on the number of transductions according to tumor type. **E** Boxplot of L1 activity with respect to smoking status (former smokers and current smokers). **F** Boxplot of the number of transductions in lung cancer patients according to ICI response evaluated at 3 months after the first ICI dose. **G** Boxplot of the number of transductions in MIBC patients according to response evaluated at the time of cystectomy. For all boxplots, differential p -values were derived by the Wilcoxon rank-sum test. The central marks represent the median, with 25th and 95th percentiles at the box, 5th and 95th percentiles at the whiskers, and minima and maxima noted by dots. ADC adenocarcinoma, NR non-responder, R responder, SCC squamous cell carcinoma

L1 activation. In addition, we noticed that most patients with high L1 activation were R, although not reaching statistical significance (p -value = 0.5804, Fig. 5F).

In the case of L1 retrotransposition in a larger MIBC cohort ($n=26$) (Table 2), we found that 57.7% of the patients presented L1 activation. We observed that all patients with high L1 activation were R (p -value = 0.026, Fig. 5G), thus following the same tendency observed in NSCLC, but this time reaching statistical significance, hence highlighting the power of L1 activation as predictive biomarker for ICI response.

Discussion

ICI have achieved a milestone in advanced cancer treatment, although the identification of response predictive biomarkers is still limited. In fact, it has become the first-line treatment for advanced NSCLC [18], recently approved for MIBC in combination with enfortumab-vedotin [19], and as neoadjuvant treatment in NSCLC [58]. In this scenario, the lack of effective predictive biomarkers of response represents a key challenge in clinical practice. In this study, we provide a wide genomic characterization for NSCLC and MIBC treated with ICI as first-line therapy.

Importantly, none of the analyzed clinical characteristics showed a statistically significant association with patient prognosis, neither in NSCLC, nor in MIBC, highlighting the need of reliable and robust genomic biomarkers for oncological patient management.

Our results confirmed that key cancer driver genes are often mutated in both R and NR patients, such as *TP53*, the most mutated gene for both tumor types, *KRAS* and *MT-CO3* in NSCLC, and *ZFH4* in MIBC. Nevertheless, we also identified specific mutations, which could potentially serve as predictive biomarkers for ICI response, such as *PIEZO2* and *MT-CO3*, specific of R and NR respectively in NSCLC patients, while *PKHD1* and *HEATR5B/WDR36* appeared exclusively in R and NR respectively in MIBC.

Moreover, by exploring the active mutational signatures in these cohorts, we found that COSMIC_4 (tobacco exposure) and COSMIC_5 were common in all NSCLC patients. The presence of the COSMIC_4, with 94% of ever-smoker patients, is expected and in agreement with what has been described for NSCLC [59, 60]. In relation to MIBC, we identified APOBEC cytidine deaminase signatures (COSMIC_13) exclusively among R patients. A correlation between APOBEC-mediated mutagenesis

and ICI effectiveness has already been described in MIBC [61], with several studies linking APOBEC mutagenesis to neoantigen generation [62, 63]. Hence, the presence of this feature could not only potentially represent a biomarker for ICI response, but also underlie the mechanisms behind this process in MIBC patients.

In relation to TMB, we detected no statistically significant association between the TMB and ICI response in NSCLC. In contrast, MIBC R patients showed a significantly higher TMB than NR patients when considering the coding regions. These results appear to indicate that WES-based estimates may be sufficient, as our WGS TMB metrics did not contribute to a higher predictive power. In any case, it should be mentioned that TMB was only found to be an effective biomarker of ICI response in MIBC.

With the aim of digging deeper into the mechanisms that could underlie ICI response, we explored the molecular pathways enriched in the sets of exclusively mutated genes in R and NR patients. We found pathways related to inflammatory response and to Ras dependent immune molecular genes exclusively mutated in NSCLC R. RAS family has been widely studied as a key regulator of the activity of multiple downstream signaling pathways, including cell proliferation [64]. In particular, oncogenic RAS mutations have been described as promoting immune evasion by favoring the expression of PD-L1 in tumor cells [65, 66], which could partly explain why ICI therapy is more effective in these patients. Similar to previous studies, we also found mutations in ERBB related pathways in R. ERBB4 alterations have been described as hampering immunotherapy response in NSCLC [67], thus promoting PD-L1 expression [67–69]. In addition, we described its co-mutation with MDM2 gene in one R patient, whose inhibition was reported to increase MHC class I and II expression in a TP53 dependent manner, its main inhibitor, and, hence, to promote neoantigen recognition and T-cell infiltration [70, 71]. Accordingly, there are different clinical trials targeting MDM2 in combination with immunotherapy [70, 72]. Finally, genes belonging to CTCF pathway, closely related to chromatin remodeling and epigenetics, presented pathogenic variants exclusively in R. Notably, CTCF has been described as an inhibitor of lncRNA responsible of reducing immunotherapy response [73].

Regarding NR patients, we found an enrichment of FGFR3 ligand binding and activation pathways. Intriguingly, FGFR3 mutations have been recently described to drive T-cell-depleted microenvironment in bladder cancer, attenuating the response to ICI in metastatic MIBC patients [74]. Moreover, we discovered an important enrichment on neural crest differentiation, which is in line with recent research pointing towards a neuronal

regulation of immune response mediated by innate lymphoid cells (ILCs) [75–77]. This is noteworthy considering the emerging field of cancer neuroscience and how ICI response could be strongly modified by neuromodulation strategies [78, 79]. We also detected exclusive alterations affecting cell-surface and cell–cell interaction components, such as integrins, and MHC class-I. In this regard, the blockage of Netrin-1, a member of one of the pathways in which these integrins are involved, has been associated to a better response to ICI [80], while MHC class-I components impairment can hamper neoantigen presentation and have been proposed as tumor resistance processes [81–83]. In addition, we identified variants more frequently in NR affecting several genes related to antigen presentation, such as HERC2, PSMD1, PSMA6, and B2M (B2M appeared also amplified in two of the patients). Our observations also indicated that an impaired HLA-I complex affects the ICI response. These results are in line with previous studies reporting recurrent inactivation of B2M in lung cancer, together with a down-regulation of the HLA-I complex, leading to an abnormal immunosurveillance in lung cancer [84]. Thus, our results confirm a molecular resistance to the ICI therapy by impairing the presentation of immunogenic neoantigens.

In MIBC patients, we found Double Strand Break Repair system alterations in R patients. Concordantly, previous studies have shown that these impairments can cause genomic instability [85, 86], PD-L1 expression and TMB upregulation, and immunotoxicity through cGAS-STING stimulation, which favor interferon expression and lymphocytes infiltration [86–89]. Furthermore, the impairment of this repair system may also trigger neoantigen generation [86, 90], favoring ICI response. In relation to this, ATM mutations have also been reported in other NSCLC cohorts in patients who responded to ICI therapy [60] while its inhibition has been described to enhance cancer immunotherapy by promoting cGAS-STING activation [91]. Among NR patients, we found a huge mutational variability, which likely indicates the activation of a mixture of molecular pathways preventing the response in a neoadjuvant scenario.

Since we are aware of the lack of the normal-matched samples in the MIBC cohort, we wanted to ensure that no specific bias was included in our results. Thus, in addition to the filtering steps explained in the Methods section, we have compared the median non-synonymous mutation rate in coding regions with those from Loriot et al. [92], a recent study that characterizes the genomic landscape of metastatic urothelial cancer performing WES of tumor and adjacent normal tissue. They reported a somatic mutation rate of 5.17 mutations/Mb which, considering the WES libraries used, equals ~260

average mutations per patient. This rate does not differ in magnitude with our results (~476). In addition, exome libraries used in their study do not cover the full range of UTR regions, which may also explain their lower mutation rate compared to ours, that include UTRs from all genes. Finally, since our results are based on the comparison between responder and non-responder patients, both groups will be affected by the same bias and the differential features identified between them should not be heavily affected.

We additionally explored features related to the tumor microenvironment by analyzing the HLA-I haplotype repertoire. In each cohort, we found several common HLA haplotypes but also identified several exclusive haplotypes to both R and NR subgroups. Stratifying patients based on this genetic background could potentially guide ICI decision-making. Specific HLA-I alleles have been already related to tumor infiltrating lymphocytes cytotoxicity activation after antigen presentation [93], and the presence of HLA-A*03 alleles has been recently suggested as a biomarker of poor response to ICI [94]. Indeed, this specific allele was found more frequently within our NR patients. HLA-A*02:01 allele was the most frequent in our cohort of MIBC, especially in NR, and has been recently associated with good prognostic in pancreatic cancer [95]. Therefore, these novel results support the need to further study the HLA haplotypes as potential predictive biomarkers for ICI response.

Finally, recent studies have reported that the activation of TEs, such as L1, can enhance ICI response by inducing inflammation and generating immunogenic neoantigens [8, 11, 96]. However, the relation between L1 activation and immunotherapy response in real-life ICI-treated patients is yet to be evaluated. Based on this and on our first results showing a higher tendency of L1 activation in tumors with higher TMB resulting in R patients, we decided to further validate the possible association between L1 activation and ICI response in extensive cohorts. In general, we found that half of the patients presented L1 activation at baseline, varying slightly among the NSCLC and MIBC patients. In NSCLC, a significant positive association was found between smoking and L1 activity, finding an association with squamous tumors, intimately linked to smoking habits. Interestingly, we detected a clear tendency in both NSCLC and MIBC, showing a higher L1 activation in R compared to NR patients, although only statistically significant in MIBC. To the best of our knowledge, this is the first time that the capacity of L1 activation was demonstrated to predict ICI response at baseline.

Conclusions

In summary, our findings highlight that while several cancer driver genes, such as *TP53*, are commonly mutated in both R and NR patients, but specific mutations were also identified as potential predictive biomarkers for ICI response. The analysis of active mutational signatures revealed interesting patterns that may relate to treatment efficacy. In this context, the relationship between TMB and ICI response resulted evident in MIBC patients but not for NSCLC. The examination of molecular pathways also indicated that certain mechanisms, such as immune evasion driven by *RAS* mutations and PD-L1 expression, play a crucial role in treatment effectiveness. Findings regarding the activation of L1 suggest a potential link between induced inflammation and response to ICI, opening new avenues for developing additional biomarkers. Ultimately, our results underscore the importance of a genomic approach in cancer management and the need for further studies to validate these biomarkers and better understand the underlying mechanisms affecting response to ICI therapy. This will not only improve clinical management for patients but also contribute to a more personalized approach in cancer treatment.

Supplementary Information

The online version contains supplementary material available at <https://doi.org/10.1186/s12967-025-06323-7>.

Supplementary Material 1: Fig. 1. A. Kaplan–Meier curves for OS with respect to ICI response for NSCLC. Patients were grouped into responders and non-responders to ICI as evaluated by CT scan 3 months after the first anti-PD1 dose. Log-rank test was used to calculate the p-value. B. Kaplan–Meier curves for OS with respect to ICI response for MIBC. Patients were grouped into responders and non-responders to ICI as evaluated at cystectomy. Log-rank test was used to calculate the p-value.

Supplementary Material 2: Fig. 2. A. Barplot showing variant allele frequency across the MIBC cohort. B. Mutational burden estimates of pre- and post-neoadjuvant immunotherapy in MIBC samples, showing the total counts per sample of INDEL and SNV variants. C. Scatterplot comparing the VAF of all the variants that are shared between the pre- and post-neoadjuvant immunotherapy in MIBC patients. D. VAF shift between exonic variants that are shared between the pre- and post-neoadjuvant immunotherapy in MIBC patients. VAF shift was calculated by subtracting the VAF of the pre-ICI sample to the VAF of the post-ICI sample. Variants whose VAF increases after neoadjuvant ICI are shown in the red scale, while variants with lower VAF after neoadjuvant ICI are shown in the blue scale.

Supplementary Material 3: Fig. 3. A. Barplot of the pathway enrichment analysis based on all the mutated genes in NSCLC responder patients. B. Barplot of the pathway enrichment analysis based on all the genes mutated in NSCLC non-responder patients. C. Barplot of the pathway enrichment analysis based on all the genes mutated in MIBC responder patients. D. Barplot of the pathway enrichment analysis based on all the mutated genes in MIBC non-responder patients.

Supplementary Material 4: Fig. 4. A. Barplot of the pathway enrichment analysis based on the 1,216 genes that are exclusively mutated in NSCLC responder patients. B. Barplot of the pathway enrichment analysis based on the 1,748 genes that are exclusively mutated in NSCLC non-responder patients. C. Barplot of the pathway enrichment analysis based on the 5,067 genes that are exclusively mutated in MIBC responder patients. D.

Barplot of the pathway enrichment analysis based on the 751 genes that are exclusively mutated in MIBC non-responder patients

Supplementary Material 5: Fig. 5. A. Boxplot of the binding affinity to the most representative HLA alleles of the peptides derived from the top-most exclusively mutated genes in NSCLC responder and non-responder patients. B. Binding affinity to the HLA-A01:01 of peptides derived from mutated *PIEZO2* and *MT-CO3*. C. Boxplot of the binding affinity to the most representative HLA alleles of the peptides derived from the top-most exclusively mutated genes in MIBC responder and non-responder patients. One-sided Wilcoxon rank-sum test was used to derive the *p*-values.

Supplementary Material 6: Fig. 6. A. Scatterplot for the correlation between the TMB calculated with all genomic variants and the LINE-1 activation measured by RetroTest for NSCLC patients. B. Scatterplot for the correlation between the TMB calculated with exonic variants and the LINE-1 activation measured by RetroTest for NSCLC patients. C. Scatterplot for the correlation between the TMB calculated with all genomic variants and the LINE-1 activation measured by RetroTest for MIBC patients. D. Scatterplot for the correlation between the TMB calculated with exonic variants and the LINE-1 activation measured by RetroTest for MIBC patients. E. Kaplan–Meier curves for OS and PFS according to durable response to ICI in NSCLC patients. The log-rank test was used to derive the *p*-values.

Supplementary Material 7.

Supplementary Material 8.

Supplementary Material 9.

Supplementary Material 10.

Supplementary Material 11.

Supplementary Material 12.

Supplementary Material 13.

Supplementary Material 14.

Supplementary Material 15.

Supplementary Material 16.

Acknowledgements

Authors thank all the enrolled patients and their families. Samples were collected and stored by the Galicia Sur Health Research Institute (IIS Galicia Sur) Biobank (registry B.0000802). This research project was made possible through the access granted by the Galician Supercomputing Center (CESGA) to its supercomputing infrastructure. The supercomputer FinisTerra III and its permanent data storage system have been funded by the Spanish Ministry of Science and Innovation, the Galician Government and the European Regional Development Fund (ERDF).

Author contributions

JB-I, MG-G, AO, MM-F contributed to the design of the study. MEL-Q, LL, LJM, CG-B, IA, LM, JMP contributed to the acquisition of the data set. JB-I, MG-G, AO, JMA, MP-G contributed to the analysis of data and their interpretation. JB-I and MM-F drafted the paper. JB-I, MG-G, AO, JMA, JMP, MM-F contributed to their interpretation and manuscript editing. All authors reviewed and revised the work and approved the final draft for submission.

Funding

This work was supported by the Instituto de Salud Carlos III (ISCIII) and the European Social Fund (“Investing in your future”) (PI19/01113) and the Spanish Association Against Cancer Scientific Foundation (IDEAS19122MART). J.B.I. was supported by the Spanish Association Against Cancer Scientific Foundation (PRDCR19007BREA_001). A.O. and M.P-G were supported by predoctoral fellowship from the Galician Innovation Agency, Xunta de Galicia (ED481A-2020/214 and IN606A-2024/017 respectively). M.P-G is currently supported by the predoctoral fellowship from Ministerio de Ciencia, Innovación y Universidades (FPU23/00744). M.M.F. was previously supported by the Spanish Association Against Cancer Scientific Foundation (INVES207MART) and is currently supported by the Miguel Servet program (CP20/00188) from the Instituto de Salud Carlos III (ISCIII) and the European Social Fund (“Investing in

your future”). M.G-G. is currently supported by a postdoctoral fellowship from the Galician Innovation Agency, Xunta de Galicia (IN606B-2024/014).

Data availability

Whole Genome Sequencing data from the NSCLC and MIBC cohorts are deposited into the Sequence Read Archive (SRA) repository under the following BioProject IDs: PRJNA1146979 and PRJNA1144206, respectively. RetroTest pipeline is publicly available at: <https://gitlab.com/mobilegenomesgroup/RETROTEST>.

Declarations

Ethics approval and consent to participate

The study was conducted with appropriate authorization from the Galician Regional Research Ethics Committee (2019/046) and from the Ethics Committee from Hospital “12 de Octubre” (17/094) following the Helsinki Declaration of 1975 and all patients signed informed consent approving their participation.

Competing interests

The authors declare no competing interests.

Author details

¹Translational Oncology Research Group, Galicia Sur Health Research Institute (IIS Galicia Sur), SERGAS-UVIGO, Estrada de Clara Campoamor, 341, 36213 Vigo, Spain. ²Mobile Genomes Lab, Centre for Research in Molecular Medicine and Chronic Diseases (CiMUS), Universidad de Santiago de Compostela, Avda, Barcelona 31, 15706 Santiago de Compostela, Spain. ³Translational Medical Oncology Group (ONCOMET), Health Research Institute of Santiago de Compostela (IDIS), Travesa da Choupana s/n, 15706 Santiago de Compostela, Spain. ⁴CINBIO, Universidade de Vigo, Vigo, Spain. ⁵Cancer Genomics Research group, Galicia Sur Health Research Institute (IIS Galicia Sur), SERGAS-UVIGO, Estrada de Clara Campoamor, 341, 36213 Vigo, Spain. ⁶Present Address: Digestive Oncology Research Group of Ourense (GIODO), Galicia Sur Health Research Institute (IIS Galicia Sur), SERGAS-UVIGO, Vigo, Spain. ⁷Present Address: Oncology Department, Complejo Hospitalario Universitario de Ourense, Calle Ramon Puga Nogueiro, 54, 32005 Ourense, Spain. ⁸Pathological Anatomy Department, University Clinical Hospital and Health Research Institute of Santiago de Compostela (IDIS), Travesa da Choupana s/n, 15706 Santiago de Compostela, Spain. ⁹Molecular and Translational Oncology Division, CIEMAT (Ed 70A), Ave Complutense 40, 28040 Madrid, Spain. ¹⁰Cell and Molecular Oncology Group Inst Inv Biomed Univ Hosp “12 de Octubre”, 28041 Madrid, Spain. ¹¹Centro de Investigación Biomédica en Red de Cáncer (CIBERONC), Madrid, Spain.

Received: 28 October 2024 Accepted: 27 February 2025

Published online: 05 April 2025

References

- Lu S, Stein JE, Rimm DL, Wang DW, Bell JM, Johnson DB, et al. Comparison of biomarker modalities for predicting response to PD-1/PD-L1 checkpoint blockade. *JAMA Oncol*. 2019;5:1195–204.
- Tsao MS, Kerr KM, Kockx M, Beasley M-B, Borczuk AC, Botling J, et al. PD-L1 immunohistochemistry comparability study in real-life clinical samples: results of blueprint phase 2 project. *J Thorac Oncol*. 2018;13:1302–11.
- Lantuejoul S, Sound-Tsao M, Cooper WA, Girard N, Hirsch FR, Roden AC, et al. PD-L1 testing for lung cancer in 2019: perspective from the IASLC Pathology Committee. *J Thorac Oncol*. 2020;15:499–519.
- Cristescu R, Mogg R, Ayers M, Albright A, Murphy E, Yearley J, et al. Pan-tumor genomic biomarkers for PD-1 checkpoint blockade-based immunotherapy. *Science* (New York NY). 2018. <https://doi.org/10.1126/science.aar3593>.
- Samstein RM, Lee C-H, Shoushtari AN, Hellmann MD, Shen R, Janjigian YY, et al. Tumor mutational load predicts survival after immunotherapy across multiple cancer types. *Nat Genet*. 2019;51:202–6.
- Büttner R, Longshore JW, López-Ríos F, Merkelbach-Bruse S, Normanno N, Rouleau E, et al. Implementing TMB measurement in clinical practice: considerations on assay requirements. *ESMO Open*. 2019;4: e000442.

7. Chan TA, Yarchoan M, Jaffee E, Swanton C, Quezada SA, Stenzinger A, et al. Development of tumor mutation burden as an immunotherapy biomarker: utility for the oncology clinic. *Ann Oncol*. 2019;30:44–56.
8. Kong Y, Rose CM, Cass AA, Williams AG, Darwish M, Lianoglou S, et al. Transposable element expression in tumors is associated with immune infiltration and increased antigenicity. *Nat Commun*. 2019;10:1–14.
9. Rodriguez-Martin B, Alvarez EG, Baez-Ortega A, Zamora J, Supek F, Demeulemeester J, et al. Pan-cancer analysis of whole genomes identifies driver rearrangements promoted by LINE-1 retrotransposition. *Nat Genet*. 2020;52:306–19.
10. Tubio JMC, Li Y, Ju YS, Martincorena I, Cooke SL, Tojo M, et al. Extensive transduction of nonrepetitive DNA mediated by L1 retrotransposition in cancer genomes. *Science*. 2014;345:1251343.
11. Shah NM, Jang HJ, Liang Y, Maeng JH, Tzeng S-C, Wu A, et al. Pan-cancer analysis identifies tumor-specific antigens derived from transposable elements. *Nat Genet*. 2023;55:631–9.
12. Yang K, Halima A, Chan TA. Antigen presentation in cancer—mechanisms and clinical implications for immunotherapy. *Nat Rev Clin Oncol*. 2023;20:604–23.
13. Han J, Dong Y, Zhu X, Reuben A, Zhang J, Xu J, et al. Assessment of human leukocyte antigen-based neoantigen presentation to determine pan-cancer response to immunotherapy. *Nat Commun*. 2024;15:1199.
14. Bray F, Laversanne M, Sung H, Ferlay J, Siegel RL, Soerjomataram I, et al. Global cancer statistics 2022: GLOBOCAN estimates of incidence and mortality worldwide for 36 cancers in 185 countries. *CA Cancer J Clin*. 2024;74:229–63.
15. Lopez-Beltran A, Cookson MS, Guercio BJ, Cheng L. Advances in diagnosis and treatment of bladder cancer. *BMJ*. 2024;384: e076743.
16. Fahmy O, Khairul-Asri MG, Schubert T, Renninger M, Malek R, Kübler H, et al. A systematic review and meta-analysis on the oncological long-term outcomes after trimodality therapy and radical cystectomy with or without neoadjuvant chemotherapy for muscle-invasive bladder cancer. *Urol Oncol*. 2018;36:43–53.
17. Reck M, Remon J, Hellmann MD. Special series: thoracic oncology: current and future therapy review articles. *J Clin Oncol*. 2022;40:586–97.
18. Hendriks LE, Kerr KM, Menis J, Mok TS, Nestle U, Passaro A, et al. Non-oncogene-addicted metastatic non-small-cell lung cancer: ESMO Clinical Practice Guideline for diagnosis, treatment and follow-up. *Ann Oncol*. 2023;34:358–76.
19. Powles T, Valderrama BP, Gupta S, Bedke J, Kikuchi E, Hoffman-Censits J, et al. Enfortumab vedotin and pembrolizumab in untreated advanced urothelial cancer. *N Engl J Med*. 2024;390:875–88.
20. Powles T, Kockx M, Rodriguez-Vida A, Duran I, Crabb SJ, Van Der Heijden MS, et al. Clinical efficacy and biomarker analysis of neoadjuvant atezolizumab in operable urothelial carcinoma in the ABACUS trial. *Nat Med*. 2019;25:1706–14.
21. Andrews S. FastQC: a quality control tool for high throughput sequence data. 2010. <http://www.bioinformatics.babraham.ac.uk/projects/fastqc/>. Accessed 15 May 2024.
22. Li H. Aligning sequence reads, clone sequences and assembly contigs with BWA-MEM. *arXiv: Genomics*. 2013.
23. Li H, Durbin R. Fast and accurate short read alignment with Burrows-Wheeler transform. *Bioinformatics (Oxford, England)*. 2009;25:1754–60.
24. Danecek P, Bonfield JK, Liddle J, Marshall J, Ohan V, Pollard MO, et al. Twelve years of SAMtools and BCFtools. *GigaScience*. 2021;10:giab008.
25. Broad Institute. Picard Tools. <http://broadinstitute.github.io/picard/>.
26. McKenna A, Hanna M, Banks E, Sivachenko A, Cibulskis K, Kernysky A, et al. The Genome Analysis Toolkit: a MapReduce framework for analyzing next-generation DNA sequencing data. *Genome Res*. 2010;20:1297–303.
27. GATK Broad Institute, Caetano-Anolles D. Somatic short variant discovery (SNVs + Indels) <https://gatk.broadinstitute.org/hc/en-us/articles/360035894731-Somatic-short-variant-discovery-SNVs-Indels>.
28. Benjamin D, Sato T, Cibulskis K, Getz G, Stewart C, Lichtenstein L. Calling somatic SNVs and Indels with Mutect2. *bioRxiv*; 2019. p. 861054. <https://www.biorxiv.org/content/https://doi.org/10.1101/861054v1>.
29. McLaren W, Gil L, Hunt SE, Riat HS, Ritchie GRS, Thormann A, et al. The ensembl variant effect predictor. *Genome Biol*. 2016;17:122.
30. Kumar P, Henikoff S, Ng PC. Predicting the effects of coding non-synonymous variants on protein function using the SIFT algorithm. *Nat Protoc*. 2009;4:1073–81.
31. Adzhubei I, Jordan DM, Sunyaev SR. Predicting functional effect of human missense mutations using PolyPhen-2. *Curr Protoc Hum Genet*. 2013. <https://doi.org/10.1002/0471142905.hg0720s76>.
32. Kandath C. mskcc/vcf2maf: vcf2maf v1.6.19. 2020. <https://doi.org/10.5281/zenodo.593251>.
33. Mayakonda A, Lin D-C, Assenov Y, Plass C, Koeffler HP. Maftools: efficient and comprehensive analysis of somatic variants in cancer. *Genome Res*. 2018;28:1747–56.
34. Lappalainen I, Lopez J, Skipper L, Hefferon T, Spalding JD, Garner J, et al. dbVar and DGVA: public archives for genomic structural variation. *Nucleic Acids Res*. 2013;41:D936–41.
35. Amemiya HM, Kundaje A, Boyle AP. The ENCODE Blacklist: identification of problematic regions of the genome. *Sci Rep*. 2019;9:9354.
36. Kumar R, Nagpal G, Kumar V, Usmani SS, Agrawal P, Raghava GPS. Hum-CFS: a database of fragile sites in human chromosomes. *BMC Genomics*. 2019;19:985.
37. Zook JM, Catoe D, McDaniel J, Van L, Spies N, Sidow A, et al. Extensive sequencing of seven human genomes to characterize benchmark reference materials. *Sci Data*. 2016;3: 160025.
38. Martincorena I, Raine KM, Gerstung M, Dawson KJ, Haase K, Van Loo P, et al. Universal patterns of selection in cancer and somatic tissues. *Cell*. 2017;171:1029–1041.e21.
39. Alexandrov LB, Kim J, Haradhvala NJ, Huang MN, Tian Ng AW, Wu Y, et al. The repertoire of mutational signatures in human cancer. *Nature*. 2020;578:94–101.
40. Priestley P, Baber J, Lolkema MP, Steeghs N, de Bruijn E, Shale C, et al. Pan-cancer whole-genome analyses of metastatic solid tumours. *Nature*. 2019;575:210–6.
41. Mermel CH, Schumacher SE, Hill B, Meyerson ML, Beroukheim R, Getz G. GISTIC20 facilitates sensitive and confident localization of the targets of focal somatic copy-number alteration in human cancers. *Genome Biol*. 2011;12:41.
42. Kuleshov MV, Jones MR, Rouillard AD, Fernandez NF, Duan Q, Wang Z, et al. Enrichr: a comprehensive gene set enrichment analysis web server 2016 update. *Nucleic Acids Res*. 2016;44:W90–97.
43. Xie Z, Bailey A, Kuleshov MV, Clarke DJB, Evangelista JE, Jenkins SL, et al. Gene set knowledge discovery with enrichr. *Curr Protoc*. 2021;1: e90.
44. Subramanian A, Tamayo P, Mootha VK, Mukherjee S, Ebert BL, Gillette MA, et al. Gene set enrichment analysis: a knowledge-based approach for interpreting genome-wide expression profiles. *Proc Natl Acad Sci*. 2005;102:15545–50.
45. Liberzon A, Birger C, Thorvaldsdóttir H, Ghandi M, Mesirov JP, Tamayo P. The Molecular Signatures Database (MSigDB) hallmark gene set collection. *Cell Syst*. 2015;1:417–25.
46. Huang R, Grishagin I, Wang Y, Zhao T, Greene J, Obenaus JC, et al. The NCATS BioPlanet—an integrated platform for exploring the universe of cellular signaling pathways for toxicology, systems biology, and chemical genomics. *Front Pharmacol*. 2019;10:445.
47. Kanehisa M, Sato Y, Furumichi M, Morishima K, Tanabe M. New approach for understanding genome variations in KEGG. *Nucleic Acids Res*. 2019;47:D590–5.
48. Kanehisa M, Furumichi M, Sato Y, Kawashima M, Ishiguro-Watanabe M. KEGG for taxonomy-based analysis of pathways and genomes. *Nucleic Acids Res*. 2023;51:D587–92.
49. Pico AR, Kelder T, van Iersel MP, Hanspers K, Conklin BR, Evelo C. WikiPathways: pathway editing for the people. *PLoS Biol*. 2008;6: e184.
50. Agrawal A, Balci H, Hanspers K, Coort SL, Martens M, Slenter DN, et al. WikiPathways 2024: next generation pathway database. *Nucleic Acids Res*. 2024;52:D679–89.
51. Ashburner M, Ball CA, Blake JA, Botstein D, Butler H, Cherry JM, et al. Gene ontology: tool for the unification of biology. The Gene Ontology Consortium. *Nat Genet*. 2000;25:25–9.

52. The Gene Ontology Consortium, Aleksander SA, Balhoff J, Carbon S, Cherry JM, Drabkin HJ, et al. The Gene Ontology knowledgebase in 2023. *Genetics*. 2023;224:iyad031.
53. Fornes O, Castro-Mondragon JA, Khan A, van der Lee R, Zhang X, Richmond PA, et al. JASPAR 2020: update of the open-access database of transcription factor binding profiles. *Nucleic Acids Res*. 2020;48:D87-92.
54. Martínez-Jiménez F, Priestley P, Shale C, Baber J, Rozemuller E, Cuppen E. Genetic immune escape landscape in primary and metastatic cancer. *Nat Genet*. 2023;55:820-31.
55. Barker DJ, Maccari G, Georgiou X, Cooper MA, Flicek P, Robinson J, et al. The IPD-IMGT/HLA Database. *Nucleic Acids Res*. 2023;51:D1053-60.
56. Jurtz V, Paul S, Andreatta M, Marcatili P, Peters B, Nielsen M. NetMHCpan 40: improved peptide-MHC class I interaction predictions integrating eluted ligand and peptide binding affinity data. *J Immunol*. 2017;199:3360-8.
57. Brea-Iglesias J, Oitaben A, Zumalave S, Rodríguez-Martin B, Gallardo-Gomez M, Santamarina M, et al. RetroTest unravels LINE-1 retrotransposition in head and neck squamous cell carcinoma. *medRxiv*; 2024. p. 2024.07.24.24310921. <https://doi.org/10.1101/2024.07.24.24310921v2>
58. Provencio M, Nadal E, González-Larriba JL, Martínez-Martí A, Bernabé R, Bosch-Barrera J, et al. Perioperative nivolumab and chemotherapy in stage III non-small-cell lung cancer. *N Engl J Med*. 2023;389:504-13.
59. Ernst SM, Mankor JM, van Riet J, von der Thüsen JH, Dubbink HJ, Aerts JGJV, et al. Tobacco smoking-related mutational signatures in classifying smoking-associated and nonsmoking-associated NSCLC. *J Thorac Oncol*. 2023;18:487-98.
60. Ravi A, Hellmann MD, Arniella MB, Holton M, Freeman SS, Naranbhai V, et al. Genomic and transcriptomic analysis of checkpoint blockade response in advanced non-small cell lung cancer. *Nat Genet*. 2023;55:807-19.
61. Shi R, Wang X, Wu Y, Xu B, Zhao T, Trapp C, et al. APOBEC-mediated mutagenesis is a favorable predictor of prognosis and immunotherapy for bladder cancer patients: evidence from pan-cancer analysis and multiple databases. *Theranostics*. 2022;12:4181-99.
62. Swanton C, McGranahan N, Starrett GJ, Harris RS. APOBEC enzymes: mutagenic fuel for cancer evolution and heterogeneity. *Cancer Discov*. 2015;5:704-12.
63. Vile RG, Melcher A, Pandha H, Harrington KJ, Pulido JS. APOBEC and cancer viroimmunotherapy: thinking the unthinkable. *Clin Cancer Res*. 2021;27:3280-90.
64. Donward J. Targeting RAS signalling pathways in cancer therapy. *Nat Rev Cancer*. 2003. <https://www.nature.com/articles/nrc969>. Accessed 8 Jul 2024.
65. Chen N, Fang W, Lin Z, Peng P, Wang J, Zhan J, et al. KRAS mutation-induced upregulation of PD-L1 mediates immune escape in human lung adenocarcinoma. *Cancer Immunol Immunother*. 2017;66:1175-87.
66. Coelho MA, de Carné TS, Rana S, Zecchin D, Moore C, Molina-Arcas M, et al. Oncogenic RAS signaling promotes tumor immunoresistance by stabilizing PD-L1 mRNA. *Immunity*. 2017;47:1083-1099.e6.
67. Cinausero M, Laprovitera N, De Maglio G, Gerratana L, Riefolo M, Macerelli M, et al. KRAS and ERBB-family genetic alterations affect response to PD-1 inhibitors in metastatic nonsquamous NSCLC. *Ther Adv Med Oncol*. 2019;11:1758835919885540.
68. Concha-Benavente F, Ferris RL. Oncogenic growth factor signaling mediating tumor escape from cellular immunity. *Curr Opin Immunol*. 2017;45:52.
69. Herrmann F, Lehr H-A, Drexler I, Sutter G, Hengstler J, Wollscheid U, et al. HER-2/neu-mediated regulation of components of the MHC class I antigen-processing pathway. *Cancer Res*. 2004;64:215-20.
70. Brummer T, Zeiser R. The role of the MDM2/p53 axis in antitumor immune responses. *Blood*. 2024;143:2701-9.
71. Ho JNHG, Schmidt D, Lowinus T, Ryoo J, Dopfer E-P, Gonzalo Núñez N, et al. Targeting MDM2 enhances antileukemia immunity after allogeneic transplantation via MHC-II and TRAIL-R1/2 upregulation. *Blood*. 2022;140:1167-81.
72. Tolcher AW, Karim R, Tang Y, Ji J, Wang H, Meng L, et al. Abstract A086: phase Ib study of a novel MDM2 inhibitor APG-115, in combination with pembrolizumab in patients with metastatic solid tumors in US. *Mol Cancer Ther*. 2019;18:086.
73. Oreskovic E, Wheeler EC, Mengwasser KE, Fujimura E, Martin TD, Tothova Z, et al. Genetic analysis of cancer drivers reveals cohesin and CTCF as suppressors of PD-L1. *Proc Natl Acad Sci*. 2022;119: e2120540119.
74. Song Y, Peng Y, Qin C, Wang Y, Yang W, Du Y, et al. Fibroblast growth factor receptor 3 mutation attenuates response to immune checkpoint blockade in metastatic urothelial carcinoma by driving immunosuppressive microenvironment. *J Immunother Cancer*. 2023;11: e006643.
75. Cardoso V, Chesné J, Ribeiro H, García-Cassani B, Carvalho T, Bouchery T, et al. Neuronal regulation of type 2 innate lymphoid cells via neuromedin U. *Nature*. 2017;549:277-81.
76. Klose CS, Artis D. Neuronal regulation of innate lymphoid cells. *Curr Opin Immunol*. 2019;56:94-9.
77. Meininger I, Carrasco A, Rao A, Soini T, Kokkinou E, Mjösberg J. Tissue-specific features of innate lymphoid cells. *Trends Immunol*. 2020;41:902-17.
78. Hanahan D, Monje M. Cancer hallmarks intersect with neuroscience in the tumor microenvironment. *Cancer Cell*. 2023;41:573-80.
79. Winkler F, Venkatesh HS, Amit M, Batchelor T, Demir IE, Deneen B, et al. Cancer neuroscience: state of the field, emerging directions. *Cell*. 2023;186:1689-707.
80. Ducarouge B, Redavid A-R, Victoor C, Chira R, Fonseca A, Hervieu M, et al. Netrin-1 blockade inhibits tumor associated myeloid-derived suppressor cells, cancer stemness and alleviates resistance to chemotherapy and immune checkpoint inhibitor. *Cell Death Differ*. 2023;30:2201-12.
81. Tong M, Wang J, He W, Wang Y, Pan H, Li D, et al. Predictive biomarkers for tumor immune checkpoint blockade. *Cancer Manag Res*. 2018;10:4501-7.
82. Sade-Feldman M, Jiao YJ, Chen JH, Rooney MS, Barzily-Rokni M, Eliane J-P, et al. Resistance to checkpoint blockade therapy through inactivation of antigen presentation. *Nat Commun*. 2017;8:1136.
83. Wang H, Liu B, Wei J. Beta2-microglobulin(B2M) in cancer immunotherapies: biological function, resistance and remedy. *Cancer Lett*. 2021;517:96-104.
84. Pereira C, Gimenez-Xavier P, Pros E, Pajares MJ, Moro M, Gomez A, et al. Genomic profiling of patient-derived xenografts for lung cancer identifies B2M inactivation impairing immunorecognition. *Clin Cancer Res*. 2017;23:3203-13.
85. Burrell RA, McClelland SE, Endesfelder D, Groth P, Weller M-C, Shaikh N, et al. Replication stress links structural and numerical cancer chromosomal instability. *Nature*. 2013;494:492-6.
86. Jiang M, Jia K, Wang L, Li W, Chen B, Liu Y, et al. Alterations of DNA damage response pathway: Biomarker and therapeutic strategy for cancer immunotherapy. *Acta Pharm Sin B*. 2021;11:2983-94.
87. Heijink AM, Talens F, Jae LT, van Gijn SE, Fehrmann RSN, Brummelkamp TR, et al. BRCA2 deficiency instigates cGAS-mediated inflammatory signaling and confers sensitivity to tumor necrosis factor-alpha-mediated cytotoxicity. *Nat Commun*. 2019;10:100.
88. Parkes EE, Walker SM, Taggart LE, McCabe N, Knight LA, Wilkinson R, et al. Activation of STING-dependent innate immune signaling by S-phase-specific DNA damage in breast cancer. *J Natl Cancer Inst*. 2017;109:djw199.
89. Zhu Y, An X, Zhang X, Qiao Y, Zheng T, Li X. STING: a master regulator in the cancer-immunity cycle. *Mol Cancer*. 2019. <https://doi.org/10.1186/s12943-019-1087-y>.
90. Riaz N, Morris L, Havel JJ, Makarov V, Desrichard A, Chan TA. The role of neoantigens in response to immune checkpoint blockade. *Int Immunol*. 2016;28:411-9.
91. Li C, Wang B, Tu J, Liu C, Wang Y, Chen J, et al. ATM inhibition enhance immunotherapy by activating STING signaling and augmenting MHC Class I. *Cell Death Dis*. 2024;15:1-14.
92. Lorient Y, Kamal M, Syx L, Nicolle R, Dupain C, Menssourri N, et al. The genomic and transcriptomic landscape of metastatic urothelial cancer. *Nat Commun*. 2024;15:8603.
93. Tran E, Robbins PF, Lu Y-C, Prickett TD, Gartner JJ, Jia L, et al. T-cell transfer therapy targeting mutant KRAS in cancer. *N Engl J Med*. 2016;375:2255-62.

94. Naranbhai V, Viard M, Dean M, Groha S, Braun DA, Labaki C, et al. HLA-A*03 and response to immune checkpoint blockade in cancer: an epidemiological study. *Lancet Oncol.* 2022;23:172–84.
95. Langtry A, Rabadan R, Alonso L, Eijck C van, Macarulla T, Lawlor RT, et al. HLA-A*02:01 allele is associated with decreased risk and a longer survival in pancreatic cancer: results from an exhaustive analysis of the HLA variation in PDAC. *medRxiv*; 2024. p. 2024.08.29.24312704. <https://www.medrxiv.org/content/https://doi.org/10.1101/2024.08.29.24312704v1>.
96. Attig J, Young GR, Hosie L, Perkins D, Encheva-Yokoya V, Stoye JP, et al. LTR retroelement expansion of the human cancer transcriptome and immunopeptidome revealed by de novo transcript assembly. *Genome Res.* 2019;29:1578–90.

Publisher's Note

Springer Nature remains neutral with regard to jurisdictional claims in published maps and institutional affiliations.